Theoretical Strength and the Onset of Plasticity in Bulk Metallic Glasses Investigated by Nanoindentation with a Spherical Indenter

H. Bei,[1,2] Z. P. Lu,[2] and E. P. George[1,2]

[1]*The University of Tennessee, Department of Materials Science and Engineering, Knoxville, Tennessee 37996-2200, USA*
[2]*Oak Ridge National Laboratory, Metals and Ceramics Division, Oak Ridge, Tennessee 37831, USA*

(Received 14 June 2004; published 16 September 2004)

The mechanical behavior of bulk metallic glasses (BMGs) was investigated by nanoindentation with a spherical indenter. The transition from perfectly elastic behavior to plastic deformation was clearly observed as a pop-in event (sudden displacement excursion) on the load-displacement curves. Hertzian stress analysis was used to describe fully the load-displacement behavior during elastic deformation and to determine the theoretical shear strengths of the BMGs.

DOI: 10.1103/PhysRevLett.93.125504 PACS numbers: 81.05.Kf, 62.20.Dc, 62.20.Fe, 81.70.Bt

The elastic limit of a defect-free solid is usually referred to as the "ideal" or "theoretical" strength. In crystalline materials, the theoretical shear strength is estimated to be on the order of $\frac{G}{10}$ [e.g., [1]], where G is the shear modulus. Crystallographic defects (e.g., dislocations) and fabrication flaws (e.g., voids) can cause yielding or fracture to occur at applied stresses that are much lower than this value. One way to minimize the influence of defects is to decrease their number: specimens in the form of thin, drawn fibers, in which the probability of finding a defect in the tested volume is very small, have traditionally been used to determine the theoretical strengths of metals [2].

Unlike crystalline metals, amorphous metals (metallic glasses) do not contain defects such as dislocations or grain boundaries; therefore, it should be easier, in principle, to experimentally determine their theoretical strengths. Furthermore, since bulk metallic glasses (BMGs) have recently been discovered [e.g., [3–7]], their mechanical properties have become easier to characterize. However, in conventional mechanical tests, such as uniaxial tensile tests, BMGs usually fracture in a catastrophic brittle manner before macroscopic yielding occurs [8–10]. Even in compression, BMGs fracture shortly after yielding (with less than 0.8% plastic strain [10]), making it difficult to unambiguously determine their yield stress. These problems are exacerbated when casting defects are present (oxides, voids, nonmelted particles, etc.), which are impossible to avoid during the fabrication of BMGs. Therefore, the details of their yielding behavior, as well as the correlation between yield point and theoretical shear strength, remain poorly understood.

Here we use nanoindentation to investigate the transition from elastic to plastic behavior in BMGs and determine their theoretical shear strengths. Nanoindentation is a useful technique for measuring the mechanical properties of small volumes of materials [11,12], including BMGs [13,14]. Typically, a Berkovich indenter, which has a pyramidal shape with triangular faces, is used in nanoindentation experiments. Unfortunately, when such an indenter is used, there is usually not a clearly discernable transition between the elastic and plastic regions on the load-displacement curves [13]. This is because with a nominally sharp indenter, the stress rises almost immediately to a value high enough to cause plastic deformation in the indented material, even at relatively small penetrations (<10 nm). To avoid this problem, we used a spherical indenter in this study which allowed us to increase the applied stress in a controlled manner and make the BMGs deform purely elastically at first and then plastically.

Two classes of BMGs were investigated: Zr-based [VIT-001 ($Zr_{41}Ti_{14}Cu_{12.5}Be_{22.5}$) and BAM11 ($Zr_{52.5}Al_{10}Ti_5Cu_{17.9}Ni_{14.6}$)] and Fe-based [(CBAM321 ($Fe_{61}Zr_8Y_2Co_6Mo_7Al_1B_{15}$) and F37 ($Fe_{61}Zr_8Y_2Co_5Cr_2Mo_7Mn_{11}B_{15}$)]. Their fabrication procedures are reported elsewhere (e.g., [3,4,15,16]). Nanoindentation experiments were performed at 23 °C using a Nanoindenter® XP (Nano Instruments Innovation Center, MTS Corporation, Knoxville, TN). Displacements (h) and loads (P) were measured with resolutions of 0.16 nm and 0.3 μN, respectively. Two geometries of diamond indenters were used: a sphere with radius $R = 1.5$ μm and, for comparison, a Berkovich indenter. The sphere radius was verified by using it to measure the modulus of fused silica which is well known [12]. The experiments were conducted in load control at a constant loading rate ($dP/dt = 50$ μN s^{-1}) to prescribed maximum loads of 1–20 mN.

Figure 1 is a typical loading and unloading P-h plot for the VIT-001 material up to a maximum load ($P_{\max}$) of 5 mN. At locations indicated by the arrows, sudden displacement excursions (pop-ins) were observed during loading, with the first pop-in occurring at a load of about 1.2 mN. Upon unloading from $P_{\max}$, the displacement is not fully recovered, indicating that a load of 5 mN causes permanent (plastic) deformation in this material. To clarify the pop-in mechanism, another loading and unloading

 © 2004 The American Physical Society

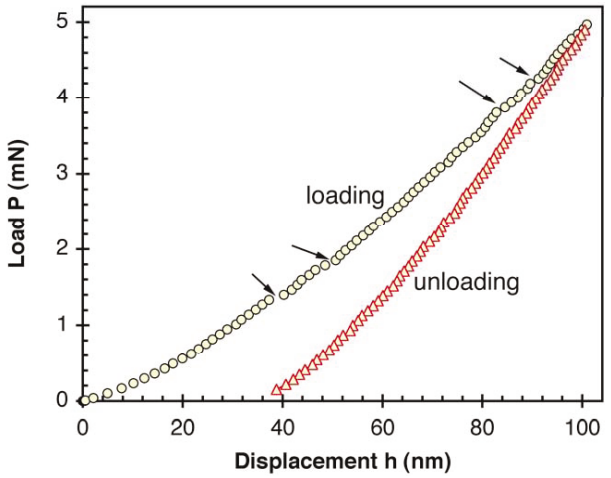

FIG. 1 (color online). Load-displacement data for VIT-001 obtained during nanoindentation with a spherical indenter showing pop-in behavior (arrows) during loading.

cycle was performed at a different location on the sample, but this time up to $P_{\max} = 1$ mN, i.e., slightly below the first pop-in load. As shown in Fig. 2, the P-h data obtained during this loading cycle are completely reversed upon unloading, indicating that the deformation is perfectly elastic up to a load of 1 mN. A power-law fit through the loading and unloading data, represented by the continuous line in Fig. 2, has the form

$$P = 0.00542\, h^{1.5}, \tag{1}$$

where the units of load P and displacement h are mN and nm, respectively.

The above expression may be compared to the general load-displacement relationship for spherical elastic contacts given by Hertz [17]:

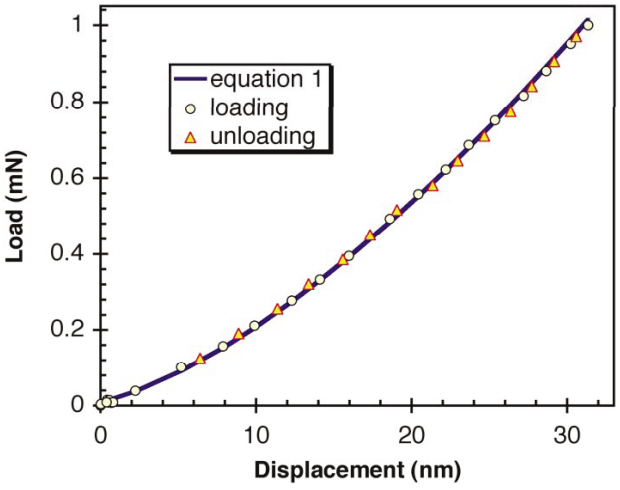

FIG. 2 (color online). Perfectly elastic loading and unloading behavior exhibited by VIT-001 below the first pop-in load. The continuous line is a power-law fit Eq. (1) to the experimental data.

$$P = \frac{4}{3} E_r \sqrt{R} h^{\frac{3}{2}} \tag{2}$$

and

$$\frac{1}{E_r} = \frac{1 - \nu_s^2}{E_s} + \frac{1 - \nu_i^2}{E_i}, \tag{3}$$

where R is the radius of the spherical indenter (1.5 μm here) and E_r is the reduced modulus, which accounts for the fact that elastic displacements occur in both the indenter and the specimen. The reduced modulus is given in terms of E_s and ν_s, the elastic modulus and Poisson's ratio of the specimens, and E_i and ν_i, the modulus and Poisson's ratio of the indenter.

For commonly used diamond indenters, the relevant elastic constants are $E_i = 1141$ GPa and $\nu_i = 0.07$ [12], and for VIT-001 they are $E_s = 101.2$ GPa and $\nu_s = 0.35$ [18]. These values can be substituted in Eq. (3) to obtain $E_r = 104.8$ GPa, which, when substituted in Eq. (2), gives the following expression for the load-displacement behavior:

$$P = 0.00541\, h^{1.5}. \tag{4}$$

The close agreement between Eqs. (1) and (4) demonstrates that during nanoindentation with a spherical diamond indenter, the load-displacement behavior of VIT-001 below the first pop-in is perfectly described by the Hertz solution for elastic contact of a sphere on a flat plate.

As an additional check of our technique, we compared the indentation modulus, $\frac{E_s}{1-\nu_s^2}$, of VIT-001 obtained from Eqs. (1)–(3), namely, 115 GPa, with that obtained using a Berkovich indenter and the Oliver-Pharr method [11]. In the latter case, the indentation modulus was determined from the unloading curve at $P_{\max} = 20$ mN and found to be 114 ± 3 GPa, which is almost identical to that determined with the spherical indenter.

Next we loaded VIT-001 up to $P_{\max} = 1.5$ mN, which is slightly higher than the first pop-in load (1.2 mN), and Fig. 3 shows the loading and unloading data. In contrast to the perfectly elastic behavior shown in Fig. 2, the loading curve in Fig. 3 is not reversed upon unloading and the displacement is not fully recovered. In other words, the specimen deforms plastically at loads higher than the first pop-in load.

The above results make it clear that the first pop-in corresponds to a transition from perfectly elastic to plastic deformation, that is, it is the onset of plasticity in VIT-001. Therefore, the maximum shear stress within the BMG, when this first pop-in occurs, represents its theoretical shear strength—if there are no defects present in the analyzed volume. To calculate this stress, we need the Hertzian elastic stress distribution underneath a spherical indenter. For the geometry shown in Fig. 4, the stress distribution within the specimen in cylindrical coordinates (r, θ, z) is given by [19]

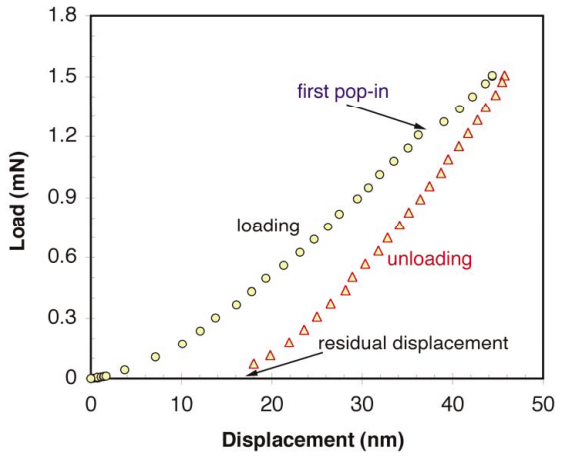

FIG. 3 (color online). Load-displacement data showing that when the VIT-001 alloy is loaded beyond the first pop-in, plastic deformation occurs and the displacement is not fully recovered upon unloading.

$$\frac{\sigma_{rr}(r,z)}{p_m} = \frac{3}{2}\left\{\frac{1-2\nu}{3}\frac{a^2}{r^2}\left[1-\left(\frac{z}{u^{1/2}}\right)^3\right] + \left(\frac{z}{u^{1/2}}\right)^3\frac{a^2u}{u^2+a^2z^2} + \frac{z}{u^{1/2}}\left[u\frac{1-\nu}{a^2+u} + (1+\nu)\frac{u^{1/2}}{a}\tan^{-1}\left(\frac{a}{u^{1/2}}\right)-2\right]\right\}, \tag{5a}$$

$$\frac{\sigma_{\theta\theta}(r,z)}{p_m} = -\frac{3}{2}\left\{\frac{1-2\nu}{3}\frac{a^2}{r^2}\left[1-\left(\frac{z}{u^{1/2}}\right)^3\right] + \frac{z}{u^{1/2}}\left[2\nu + u\frac{1-\nu}{a^2+u} - (1+\nu)\times\frac{u^{1/2}}{a}\tan^{-1}\left(\frac{a}{u^{1/2}}\right)\right]\right\}, \tag{5b}$$

$$\frac{\sigma_{zz}(r,z)}{p_m} = -\frac{3}{2}\left(\frac{z}{u^{1/2}}\right)^3\left(\frac{a^2u}{u^2+a^2z^2}\right), \tag{5c}$$

$$\frac{\tau_{rz}(r,z)}{p_m} = -\frac{3}{2}\left(\frac{rz^2}{u^2+a^2z^2}\right)\left(\frac{a^2u^{1/2}}{a^2+u}\right), \tag{5d}$$

where

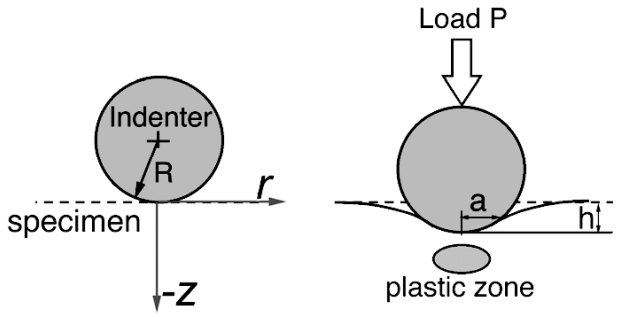

FIG. 4. Geometry of axisymmetric spherical indentation.

$$u = \frac{1}{2}\left\{(r^2+z^2-a^2) + [(r^2+z^2-a^2)^2 + 4a^2z^2]^{1/2}\right\}, \tag{5e}$$

a is the contact radius given by

$$a = \sqrt{Rh}, \tag{5f}$$

and p_m is the mean pressure given by

$$p_m = \left(\frac{16PE_r^2}{9\pi^3R^2}\right)^{1/3}. \tag{5g}$$

At each point in the specimen, the components of the stress tensor, σ_{rr}, $\sigma_{\theta\theta}$, σ_{zz}, and τ_{rz} [Eq. (5)) can be used to calculate the three principal stresses σ_1, σ_2, and σ_3, from which a local maximum shear stress can be obtained as a function of position:

$$\tau_{\max}(r,z) = \frac{\sigma_1 - \sigma_3}{2}. \tag{6}$$

Figure 5 shows a contour plot of $\tau_{\max}$ as a function of position within the specimen. The magnitude of $\tau_{\max}$ varies from point to point within the specimen, but it reaches a peak, τ_{crit}, directly below the center of the spherical indenter ($r = 0$) at a distance of about half the contact radius (a) below the specimen surface, i.e.,

$$\tau_{\text{crit}} = 0.445p_m @ r = 0, \qquad z \approx 0.5a. \tag{7}$$

Using Eqs. (5g) and (7), it is found that $\tau_{\text{crit}} = 3.1$ GPa for the VIT-001 material. This τ_{crit} is defined here as the theoretical shear strength. As mentioned earlier, the theoretical shear strength of crystalline materials is on the order of $\frac{G}{10}$ [1], where G is the shear modulus. Similar estimates are not available for amorphous materials, but if we assume that it is the same for BMGs, then the theoretical shear strength of VIT-001 should be ~3.7 GPa based on its reported shear modulus of 37.4 GPa [18]. This is close to the value calculated above for τ_{crit}, indicating that the load at first pop-in, during nanoindentation with a spherical indenter, can be used to obtain realistic values for the theoretical shear strength of BMGs.

It is worth noting that the τ_{crit} obtained above is significantly larger than the critical shear stress (~0.85 GPa) calculated from the reported uniaxial compressive strength of VIT-001 (1.7 GPa [10]). This is probably because our nanoindentation experiments probe very small volumes of materials (~30 nm penetration depth at the first pop-in), which are likely to be defect free. In contrast, relatively large volumes of material are tested in conventional tension/compression tests. Casting defects such as oxides, voids, and unmelted particles are usually present in BMGs. These defects are more likely to be present in the gage sections of tension/compression specimens than in the volumes analyzed by nanoindentation, and therefore more likely to influence the latter experiments. As a result, the τ_{crit} measured by us is higher than

TABLE I. Mechanical properties of the bulk metallic glasses investigated in this study.

	VIT-001	BAM11	CBAM321	F37
Indentation modulus, sphere[a] (GPa)	115	109	222	217
Indentation modulus, Berkovich[b] (GPa)	114	107	231	223
Load at first pop-in (mN)	1.2	1.1	2.2	2.6
Max. shear stress at first pop-in[c] (GPa)	3.1	2.9	5.5	5.7
Yield stress, shear[d](GPa)	~0.85	~0.82	...	...

[a] Calculated from Eqs. (2) and (3)
[b] Determined using the Oliver-Pharr method [11]
[c] Calculated from Eqs. (5g) and (7)
[d] Calculated from the uniaxial compressive yield stress [8,9]

the maximum shear stress measured in tension/compression tests and more closely approaches the theoretical strength of BMGs.

Pop-ins and elastic-to-plastic transitions similar to those observed in VIT-001 were also observed in the other three BMGs, indicating that nanoindentation with a spherical indenter is a good technique to determine the critical shear stress corresponding to the onset of plasticity in BMGs. Table I summarizes the indentation modulus, load at first pop-in, and the maximum shear stress at first pop-in for the BMGs investigated in this study. The Fe-based BMGs have higher modulus and strength than the Zr-based alloys, suggesting that the former alloys are intrinsically stronger than the latter.

In summary, two Zr-based and two Fe-based BMGs were investigated by nanoindentation with a spherical indenter. Sudden displacement excursions (pop-ins) were observed in all four BMGs during loading. The first of these pop-ins marked the transition from perfectly elastic to plastic deformation, i.e., it indicated the onset of plastic flow (incipient plasticity) in these materials.

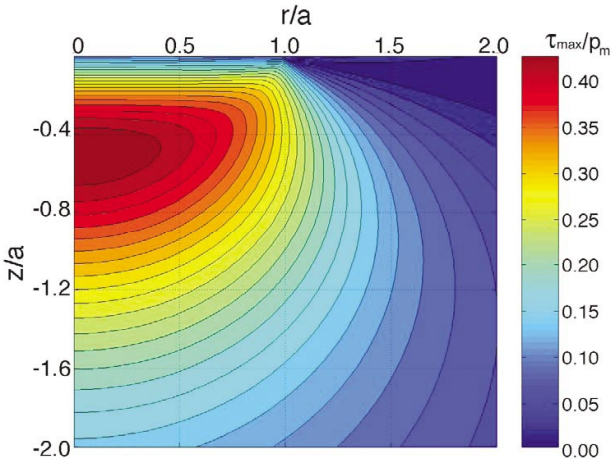

FIG. 5 (color online). Contour plot showing the distribution of τ_{max} in VIT-001. The peak value of shear stress, τ_{crit}, occurs directly below the center of the spherical indenter ($r = 0$) at a distance of about half the contact radius (a) below the specimen surface.

Hertzian stress analysis was used to calculate the maximum shear stress in the materials when the first pop-in occurred, allowing us to experimentally determine the theoretical or ideal strengths of the BMGs.

This research was sponsored by the Division of Materials Sciences and Engineering, Office of Basic Energy Sciences, U.S. Department of Energy under Contract No. DE-AC05-00OR22725 with UT-Battelle, LLC.

[1] G. E. Dieter, *Mechanical Metallurgy* (McGraw-Hill, New York, 1986), p. 119.
[2] S. S. Brenner, J. Appl. Phys. **27**, 1484 (1956).
[3] W. L. Johnson, JOM-J. Min. Met. Mat. S. **54**, 40 (2002).
[4] A. Inoue, in *Bulk Amorphous Alloys: Practical Characteristics and Applications* (Trans Tech Publications Ltd., Switzerland, 1999).
[5] Z. P. Lu, C. T. Liu, J. R. Thomos, and W. D. Porter, Phys. Rev. Lett. **92**, 245503 (2004).
[6] A. Inoue and X. M. Wang, Acta Mater. **48**, 1383 (2000).
[7] T. D. Shen and R. B. Schwarz, Appl. Phys. Lett. **75**, 45 (1999).
[8] C. T. Liu *et al.*, Metall. Mater. Trans. A **29**, 1811 (1998).
[9] J. Lu, G. Ravichandran, and W. L. Johnson, Acta Mater. **51**, 3429 (2003).
[10] Z. F. Zhang, J. Eckert, and L. Schultz, Acta Mater. **51**, 1167 (2003).
[11] W. C. Oliver and G. M. Pharr, J. Mater. Res. **7**, 1564 (1992).
[12] J. L. Hay and G. M. Pharr, in *ASM Handbook Vol. 8: Mechanical Testing and Evaluation*, edited by H. Kuhn, and D. Medkin (ASM International, Materials Park, OH, 2000).
[13] R. Vaidyanathan, M. Dao, G. Ravichandran, and S. Suresh, Acta Mater. **49**, 3781 (2001).
[14] C. A. Schuh and T. G. Nieh, J. Mater. Res. **19**, 46 (2004).
[15] Z. P. Lu, C. T. Liu, and W. D. Porter, Appl. Phys. Lett. **83**, 2581 (2003).
[16] Z. P. Lu, C. T. Liu, C. A. Carmichael, W. D. Porter, and S. C. Deevi, J. Mater. Res. **19**, 921 (2004).
[17] K. L. Johnson, *Contact Mechanics* (Cambridge University Press, Cambridge, England, 1985), p. 92.
[18] Y. Zhang *et al.*, J. Mater. Res. **16**, 1675 (2001).
[19] C. Anthony and C. Fischer, *Introduction to Contact Mechanics* (Springer, New York, 2000), p. 89.